Systemic inflammation suppresses lymphoid tissue remodelling and B cell immunity during concomitant local infection

Yannick O Alexandre[1], Sapna Devi[1,2], Simone L Park[1], Laura K. Mackay[1,2], William R. Heath[1,2], Scott N. Mueller[1,2]*

[1]Department of Microbiology and Immunology, The University of Melbourne, The Peter Doherty Institute for Infection and Immunity, Melbourne, Victoria 3000, Australia.

[2]The Australian Research Council Centre of Excellence in Advanced Molecular Imaging, The University of Melbourne, Melbourne, Victoria 3000, Australia.

* To whom correspondence may be addressed. Email: smue@unimelb.edu.au

Keywords: Inflammation, pathogen coinfection, immune response; B cells; lymphoid stromal cells.

Abstract

Concurrent infection with multiple pathogens occurs frequently in individuals and can result in exacerbated infections and altered immunity. However, the impact of such coinfections on immune responses remains poorly understood. Here we reveal that systemic infection results in an inflammation-induced suppression of local immunity. During localized infection or vaccination in barrier tissues including the skin or respiratory tract, concurrent systemic infection induces a type I interferon-dependent lymphopenia that impairs lymphocyte recruitment to the draining lymph node (dLN). This leads to suppressed lymphoid stromal cell expansion and dLN remodelling and impaired induction of B cell responses and antibody production. Our data suggest that contemporaneous systemic inflammation constrains the induction of regional immunity.

36 **Introduction**

37

38 Viral pathogens that infect the skin and mucosa, including herpes simplex virus (HSV) and
39 influenza viruses, induce immune responses in lymph nodes (LN) that drain the site of local
40 infection. Induction of immune responses relies upon effective recruitment of B cells and T
41 cells from the circulation where they can encounter cognate viral antigens presented by
42 professional antigen presenting cells. Coordinated cellular interactions define T and B cell
43 activation, proliferation and differentiation, and these interactions are supported by specialized
44 microanatomical compartments within LNs [1]. Networks of non-hematopoietic lymphoid
45 stromal cells (LSCs) construct the microarchitecture of LNs, providing both structural and
46 functional support for the induction of immune responses. Lymphatic endothelial cells (LEC)
47 form the afferent and efferent lymphatic vessels required for sampling peripheral tissues and
48 exit of lymphocytes back to the blood circulation, respectively. Lymphocytes that enter the LN
49 from the blood are recruited via specialized blood endothelial cells (BEC) that form $PNAd^+$
50 high endothelial venules (HEV) [2].

51 Subsets of mesenchymal fibroblastic reticular cells (FRC) construct the LN architecture and
52 include marginal reticular cells (MRC), follicular dendritic cells (FDC), T cell zone FRC and
53 additional reticular cells localized in B cell follicles. FRC are identified on the basis of
54 expression of podoplanin (PDPN; also called gp38) and lack expression of the endothelial cell
55 marker CD31. FRC respond dynamically to inflammation by modulating their gene expression
56 program that influences immune responses [3, 4]. This includes down-regulation of the expression
57 of the chemokines CCL19 and CCL21 and up-regulation of CXCL10, which affects the
58 positioning of leukocytes that regulate CD8 and CD4 T cell responses [5, 6]. The importance of
59 the mesenchymal LSC network was demonstrated in studies showing that depletion of the FRC
60 network results in impaired induction of immune responses [7, 8].

61 Localized infections induce considerable enlargement of the LNs, including recruitment and
62 proliferation of lymphocytes and expansion of stromal cell networks. T cell responses are
63 initiated rapidly within LNs, with activation and proliferation of pathogen-specific T cells
64 occurring in as little as 2 days, followed by egress of the expanded pool of effector cells after
65 5-6 days. B cell responses are initiated with similar rapidity, and B cells differentiate into short-
66 lived antibody secreting cells (ASC) within days, while other B cells migrate to B cell follicles
67 to form germinal centers (GC) and differentiate into high affinity plasma blasts (PB) or memory
68 B cells. GCs form within days after infection but can persist for weeks or months. Notably, LN

69 expansion peaks 1-2 weeks after infection, which is delayed relative to the induction of T cell
70 responses, suggesting that remodelling of LN stromal cell networks may be particularly
71 important for supporting B cell responses. We have previously shown that LN enlargement
72 after HSV infection requires recruitment of lymphocytes from the circulation to induce LN
73 expansion, while B cells are required to sustain stromal cell responses [4].

74 The process of immune response generation in LNs draining the site of localized infection with
75 a single pathogen is well characterized. However, people are often infected with multiple
76 pathogens simultaneously, and such pathogen coinfections can substantially modulate immune
77 responses and the outcomes of infections [9, 10]. Yet, the mechanisms underlying altered
78 immunity during pathogen coinfections remains poorly understood. Here we investigated the
79 impact of systemic coinfection on LN remodelling and immune response generation following
80 localized viral infection. Both systemic coinfection of mice with lymphocytic choriomeningitis
81 virus (LCMV) and the induction of systemic inflammation, impaired LN swelling and LSC
82 expansion and inhibited B cell responses to localized infection. We show that systemic
83 inflammation induces a type I interferon (IFN-I) dependent lymphopenia, thereby impairing
84 the recruitment of B cells to draining LNs and hindering the induction of humoral immune
85 responses.

86

87

88

Results

Restrained LN remodelling and suppressed B cell responses after LCMV infection.

To investigate how different viral pathogens influence lymphoid tissue remodelling, we infected mice subcutaneously in the footpad with HSV or LCMV Armstrong and enumerated stromal cell populations in the draining popliteal LN (pLN) by flow cytometry 8 days after infection (Fig. 1A). HSV inoculation results in an infection that remains localized to tissues near the site of inoculation [4], whereas LCMV replicates locally as well as spreading systemically, including to the spleen [11, 12]. HSV infection induced a marked increase in total pLN cellularity and expanded all populations of pLN LSC: PDPN$^+$ FRC, PDPN$^+$ CD31$^+$ LEC, CD31$^+$ BEC and CD31$^+$ PNAd$^+$ HEV (Fig. 1B). In contrast, LCMV infection resulted in only a marginal increase in cellularity and no significant expansion of the subsets of LSC in the LN compared to uninfected mice (Fig. 1B).

Examination of pLN by confocal microscopy revealed substantial enlargement of the draining LN after HSV infection, whereas pLN were small and lacked organized B cell zones after LCMV infection (Fig. 1C). Closer examination revealed substantial disorganisation of the PDPN$^+$ T cell zone FRC network that ensheaths laminin$^+$ reticular fibers (Fig. 1D) and loss of B cell zone stromal cell organisation after LCMV infection (Fig. 1E). Notably, in LCMV infected mice B cell follicles were highly disorganized, and we could not detect FDC, whereas B cell follicle organisation and FDCs were intact in HSV infected mice (Fig. 1E). Moreover, we observed the formation of a network of PDPN$^+$ FRC on the capsular side of the B cell follicles in LCMV infected mice (Fig. 1E, yellow arrows). This indicated that the B cell follicles retracted from the LN capsule and a population of subcapsular PDPN$^+$ FRC formed in this zone during LCMV infection.

Because MAdCAM-1$^+$ MRC form a specialized stromal layer between B cell follicles and the subcapsular sinus, we postulated that the expanded subcapsular LSC in LCMV infected mice might be MRC, but subsequent analysis revealed that MAdCAM-1$^+$ were not expanded following LCMV infection. Conversely, we observed a substantial increase in MAdCAM-1$^+$ PDPN$^+$ FRC after HSV infection, but not after LCMV infection (Fig. 1F). Greater than half of all FRC were MAdCAM-1$^+$ after HSV infection (Fig. 1G), suggesting that expression of this adhesion molecule was upregulated after HSV but not LCMV infection. Staining of tissue sections confirmed increased expression of MAdCAM-1 on T cell zone FRC in pLN after HSV but not LCMV infection (Fig. S1). This suggests that MAdCAM-1, which is typically used to

define MRC and is also expressed by FDC in LNs, is not a reliable marker of MRC after infection.

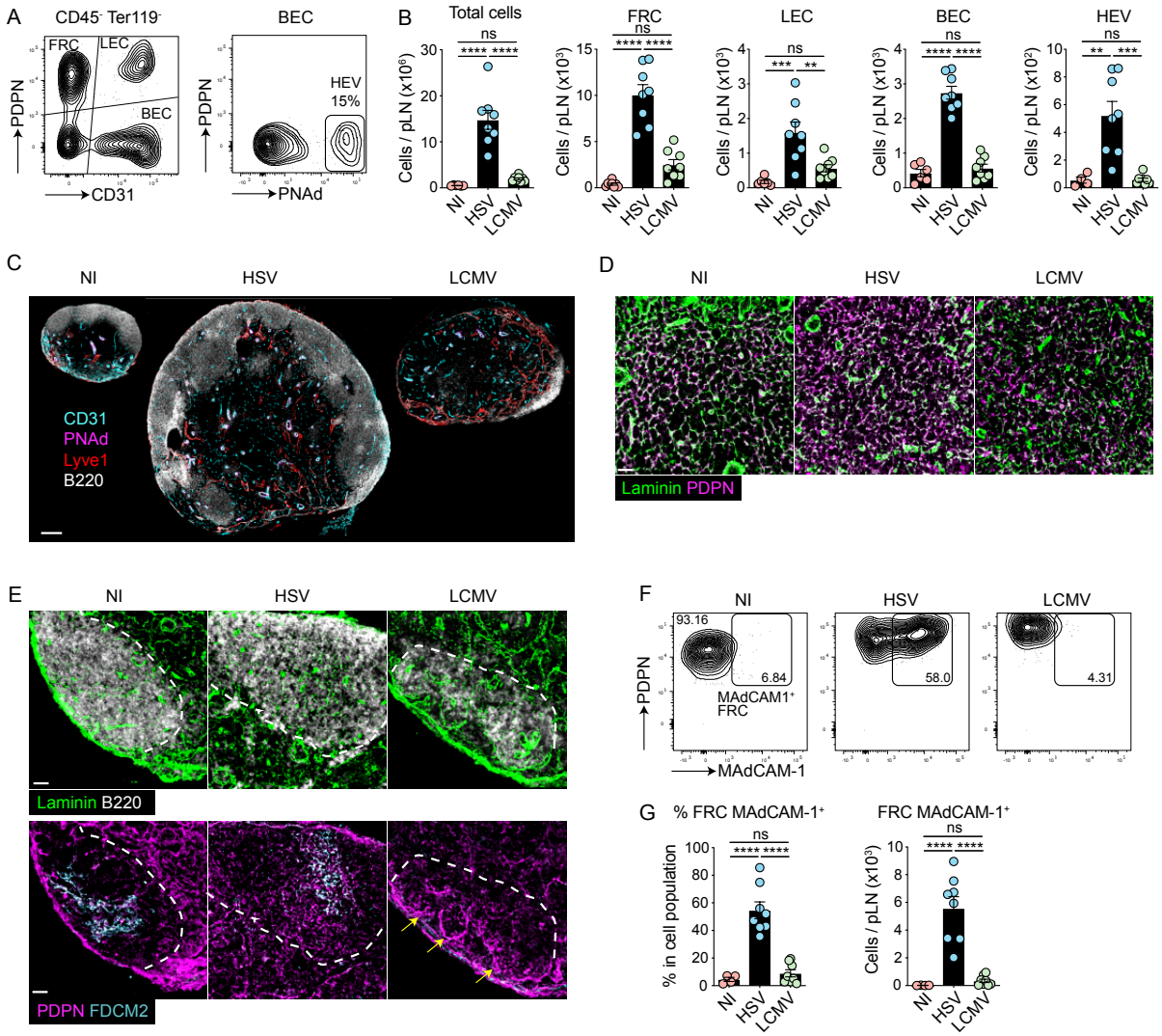

Fig. 1. Restrained remodelling of the draining LN during LCMV infection. (A) Gating strategy to identify CD45$^-$ Ter119$^-$ stromal cell subsets by flow cytometry. (B) Numbers of total cells and stromal cell subsets in the pLN from uninfected (NI) mice and mice infected s.c. with HSV or LCMV analysed by flow cytometry. Graphs show pooled data (mean ± SEM) from 3 independent experiments each with 2-3 mice per group. *P < 0.05, **P < 0.01, *** P < 0.001, ****P < 0.0001, ns, non-significant, by ANOVA with Tukey's multiple comparisons test. (C-E) pLN sections from NI, HSV or LCMV infected mice were stained for B220, Lyve1, CD31 and PNAd (C), laminin and podoplanin (D) or laminin, B220, podoplanin, amd FDC-M2 (E) and analysed by confocal microscopy. Data are representative of 2 experiments with 3 mice per group. Dotted lines depict border of B cell follicles and arrows show subcapsular FRC in LCMV pLN that were not observed in NI or HSV pLN. Scale bars, 200µm (C), 30µm (D-E) (F) MAdCAM-1 expression on FRC from NI mice and following HSV or LCMV infection. (G) Percentage and numbers of MAdCAM-1$^+$ FRC in the pLN of NI and mice infected s.c. with HSV or LCMV. Graphs show pooled data (mean ± SEM) from 3 independent experiments each with 2-3 mice per group. ****P < 0.0001, ns, non-significant, by ANOVA with Tukey's multiple comparisons test.

Next, we examined virus-specific CD8$^+$ T cell responses in the pLN by major histocompatibility complex class I (MHC-I) tetramer staining. Local infection with LCMV induced larger numbers of virus-specific CD8$^+$ T cells compared to HSV infection (Fig. 2A-B). In contrast, we found that B cell numbers were significantly reduced in draining pLN after LCMV infection in comparison with HSV infected mice (Fig. 2D). Expansion of GL7$^+$ germinal center (GC) B cells and CD138$^+$ antibody secreting cells (ASC) was also significantly lower in the pLN after LCMV infection compared to HSV infection (Fig. 2C-E). B cell follicles were increased in size after HSV infection and contained GL7$^+$ GC B cells, while B cell follicles were markedly reduced in size and GL7$^+$ cells were extrafollicular in LCMV infected mice (Fig. 2F). Large numbers of CD138$^+$ ASC accumulated at the border between T and B cell zones and within the medullary cords after HSV infection, whereas ASC were reduced and only observed in the medulla during LCMV infection (Fig. 2F). Thus, LCMV infection results in impaired LN remodelling, loss of B cell follicles and restrained B cell responses in draining LN.

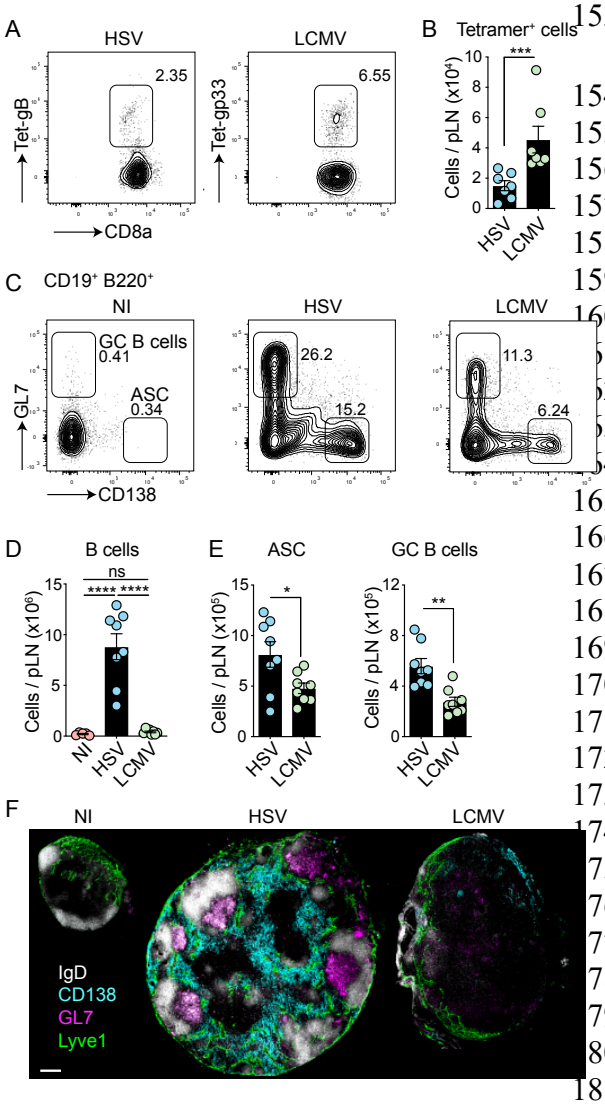

Fig. 2. Suppressed B cell responses during LCMV infection. (A) Tetramer staining of CD8$^+$ T cells, following HSV and LCMV infection. (B) Numbers of CD8$^+$ Tetramer$^+$ cells in the pLN of HSV and LCMV-infected mice. Data are pooled from 2 independent experiments with 3-4 mice per group. ***P < 0.001, by Mann-Whitney test. (C) Flow cytometry analysis of GL7$^+$ GC B cells and CD138$^+$ ASC. B cells were first gated on live CD19$^+$ CD3$^-$ NK1.1$^-$ cells. (D) Absolute numbers of B cells in the popliteal LN from NI mice and mice infected with HSV or LCMV. Graphs show pooled data (mean ± SEM) from 3 independent experiments each with 2-3 mice per group. ****P < 0.0001, ns, non-significant, by ANOVA with Tukey's multiple comparisons test. (E) ASC and GC B cells in the pLN from mice infected with HSV or LCMV. Graphs show pooled data (mean ± SEM) from 2 independent experiments each with 4 mice per group. *P < 0.05, **P < 0.01, by unpaired two-tailed t test. (F) pLN sections from NI, HSV or LCMV

182 infected mice were stained for IgD, CD138, GL7 and Lyve1 and analysed by confocal
183 microscopy. Data are representative of 2 experiments with 3 mice per group. Scale bar, 200μm.
184

185 *LCMV coinfection suppresses LN remodelling in response to localized infection.*

186 The subdued stromal cell expansion and altered lymphoid tissue architecture observed
187 following LCMV infection led us to investigate the impact of LCMV infection on LN
188 remodelling during localized HSV coinfection. We infected mice with HSV in the footpad and
189 coinfected the mice 2 days later with LCMV either by the same route or systemically by
190 intraperitoneal infection (Fig. 3A). LCMV coinfection by either route markedly restrained the
191 increase in pLN cellularity induced by HSV infection and suppressed FRC expansion (Fig.
192 3B). Local infection with LCMV resulted in infection of pLN FRC whereas systemic LCMV
193 infection did not (Fig. S2A). Yet, both routes of infection resulted in equivalent suppression of
194 the draining LN response (Fig. 3B), ruling out an inhibitory role of LCMV through direct
195 infection of FRC. Since local LCMV infection also results in systemic spread of virus from the
196 LN to spleen [11], we performed subsequent experiments using systemic LCMV coinfection.
197 Importantly, LCMV coinfection did not alter the growth of HSV in the tissue (Fig. 3C).

198 We examined HSV-draining pLN sections by confocal microscopy and discovered that LCMV
199 coinfection prominently altered pLN remodelling in response to HSV. In coinfected mice B
200 cell follicles were small and disorganized and LYVE-1^{+} medullary sinuses were more
201 prominent compared to mice infected with HSV alone (Fig. 3D). Closer examination of B cell
202 follicles in coinfected mice revealed fewer B cells, reduction of the FDC network within the
203 follicles and recession of the follicles away from the pLN subcapsular sinus (Fig. 3E).
204 Strikingly, a dense network of PDPN^{+} FRC formed between B cell follicles and the pLN
205 capsule in coinfected mice (Fig. 3E, yellow arrows), similar to what we observed during local
206 LCMV infection (Fig. 1E), that was absent from mice infected with HSV alone.

207 Quantification of cells by flow cytometry revealed a significant reduction in total cellularity
208 and reduced expansion of pLN FRC, LEC, BEC and PNAd^{+} HEV in HSV-draining LN from
209 LCMV coinfected mice (Fig. 3F). Coinfection suppressed the induction of MAdCAM-1 on
210 FRC (Fig. 3G), resulting in a significant reduction in both MAdCAM-1^{+} as well as MAdCAM-
211 1^{-} FRC (Fig. S2B). We also examined CD157 (BP-3) expression on FRC, a marker that has
212 been used to identify subpopulations of FRC including CD157-lo medullary FRC [13]. Both
213 CD157^{+} T cell zone FRC and CD157-lo medullary FRC populations were reduced in the pLN

214 of mice coinfected with HSV and LCMV in comparison with mice infected with HSV alone

215 (Fig. 3H).

216

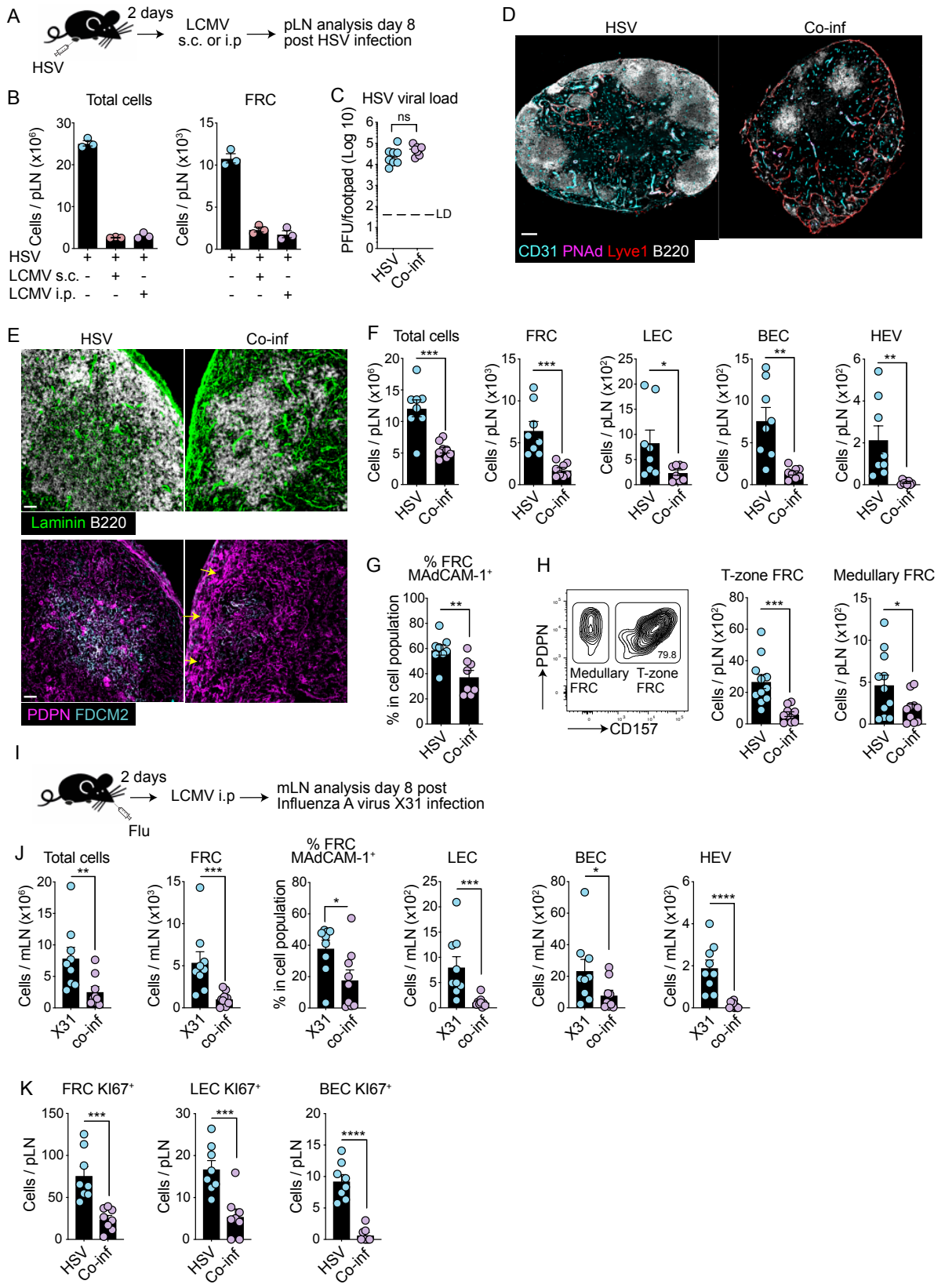

217

218 **Fig. 3. LCMV coinfection suppresses lymphadenopathy to localized infection.** (A)
219 Experimental schematic of coinfection. Mice were infected subcutaneously (s.c.) with HSV
220 and 2 d later infected with LCMV s.c. or intraperitoneally (i.p.). pLN were analysed 8 d post
221 HSV infection. (B) Numbers of total cells and FRC in the pLN of infected mice analysed by
222 flow cytometry. Graphs are representative of 2 experiments with 2-3 mice per group (mean ±
223 SEM). (C) HSV viral load in the footpad of infected mice. Mice were infected as in A and
224 footpad tissue harvested 5 d post-HSV infection for plaque assay. Data are pooled from 2
225 independent experiments with 4 mice per group. ns, non-significant, by Mann-Whitney test
226 LD: limit of detection. (D-E) pLN sections from NI, HSV or coinfected mice were stained for
227 B220, Lyve1, CD31, and PNAd (D), Laminin, B220, podoplanin, and FDC-M2 (E) and
228 analysed by confocal microscopy. Data are representative of 2 experiments with 3 mice per
229 group. Scale bar, 40μm. (F-G) Numbers of total cells and stromal cell subsets (F) and
230 MAdCAM-1 expression analysis on FRC (G) in the pLN of HSV and coinfected mice analysed
231 by flow cytometry. Graphs show pooled data (mean ± SEM) from 2 independent experiments
232 with 4 mice per group. (H) Expression of CD157 on PDPN^{+} CD31^{-} MAdCAM-1^{-} CD21/35^{-}
233 cells to define T cell zone FRC (CD157^{+}) and medullary FRC (CD157^{-}) by flow cytometry.
234 Graphs are pooled data of 3 experiments with 2-4 mice per group (mean ± SEM). *P < 0.05,
235 **P < 0.01, *** P < 0.001, ****P < 0.0001, by unpaired two-tailed t test (F-H). (I) Mice were
236 infected intranasally with Flu-gB and 2 d later infected systemically with LCMV. Mediastinal
237 LN (medLN) were analysed 8 d post Flu infection. (J) Numbers of total cells, stromal cell
238 subsets, and MAdCAM-1 expression analysis on FRC in the medLN of Flu and coinfected
239 mice analysed by flow cytometry. Graphs show pooled data (mean ± SEM) from 2 independent
240 experiments with 4-5 mice per group. *P < 0.05, **P < 0.01, *** P < 0.001, ****P < 0.0001,
241 by Mann-Whitney test. (K) Proliferation of stromal cell subsets following HSV and
242 coinfection. Mice were infected as in A and pLN harvested 5 d post-HSV infection and
243 intracellular KI67 expression was analysed flow cytometry. Graphs show pooled data (mean ±
244 SEM) from 2 independent experiments each with 4 mice per group. *** P < 0.001, ****P <
245 0.0001, by unpaired two-tailed t test.
246

247 These data suggested that LCMV coinfection inhibited LN expansion in response to local HSV
248 infection. To determine if systemic coinfection also suppressed dLN responses to other
249 localized infections, we infected mice intranasally with Influenza A virus X31 and coinfected
250 these mice with LCMV 2 days later (Fig. 3I). Coinfection suppressed immune responses in the
251 draining mediastinal LNs (mLN), resulting in reduced cellularity and impaired expansion of
252 FRC, LEC, BEC and PNAd^{+} HEV, as well as impaired upregulation of MAdCAM-1 by mLN
253 FRC compared to mice infected with influenza alone (Fig. 3J). This indicated that systemic
254 infection concurrent with either a skin or respiratory viral infection suppresses immune
255 responses in the LN draining the site of localized challenge.

256 Since systemic coinfection suppressed expansion of pLN LSC, we wanted to know if this was
257 due to reduced proliferation or altered survival of LSC. We examined proliferating LSC in
258 LCMV and HSV coinfected mice by staining for Ki67. Significantly fewer Ki67^{+} FRC, LEC
259 and BEC were detected in coinfected mice when compared to mice infected with HSV alone

260 (Fig. 3K). In contrast, coinfection did not alter the number of apoptotic (Annexin-V+ PI+)
261 FRC, LEC or BEC compared to that observed following infection with HSV alone (Fig. S2C).
262 Further, we observed no alterations in metabolic functions as determined by glucose or lipid
263 uptake, mitochondrial mass or oxidative stress in pLN LSC in coinfected mice compared to
264 mice infected with HSV alone (Fig. S2D-E). Thus, systemic LCMV coinfection suppressed
265 dLN remodelling and stromal cell expansion in response to localized infection.

266

267 *Systemic coinfection suppresses B cell responses to localized infection*

268 We examined immune responses in HSV and LCMV coinfected mice and observed that
269 although total numbers of $CD8^+$ T cells in the pLN were reduced by coinfection, HSV-specific
270 $CD8^+$ T cell responses were unaffected (Fig. 4A). Systemic LCMV coinfection also reduced
271 the accumulation of total $CD4^+$ T cells in the draining pLN and suppressed the induction of T
272 follicular helper (T_{FH}) cells compared to mice infected with HSV alone (Fig. 4B, S3A). B cell
273 numbers were significantly reduced in the pLN of coinfected mice and the induction of GC B
274 cells and ASCs was impaired (Fig. 4C). This suppression of local B cell responses during
275 LCMV coinfection was not due to increased apoptosis of B cells or T cells, as indicated by
276 AnnexinV staining (Fig. 4D). Histological examination of pLN sections revealed a reduction
277 in the size and numbers of $GL7^+$ GC B cells and fewer $CD138^+$ plasma cells in coinfected mice
278 (Fig. 4E). Moreover, systemic LCMV coinfection significantly suppressed HSV-specific
279 antibody responses (Fig. 4F).

280 To investigate the impact of systemic coinfection on the induction of local antigen-specific B
281 cell responses, we examined ovalbumin (OVA)-specific B cell receptor transgenic OB-I B cell
282 responses following transfer into B6 mice and immunization with OVA in complete freunds
283 adjuvant (OVA/CFA) (Fig, 4G). OB-I B cells expanded significantly in the pLN following
284 sub-cutaneous OVA/CFA immunization and formed GC B cells and ASCs (Fig. 4H and Fig
285 S3B). Coinfection of mice with LCMV significantly impaired the expansion of the OB-I B
286 cells in the pLN, reduced the number of GC cells and ASCs and reduced the frequency of OB-
287 I B cells that developed into GC cells and ASCs (Fig. 4H and Fig. S3B). Together, these data
288 show that systemic coinfection with an unrelated pathogen suppresses the induction of antigen-
289 specific B cell responses in LN draining the site of a localized challenge.

290

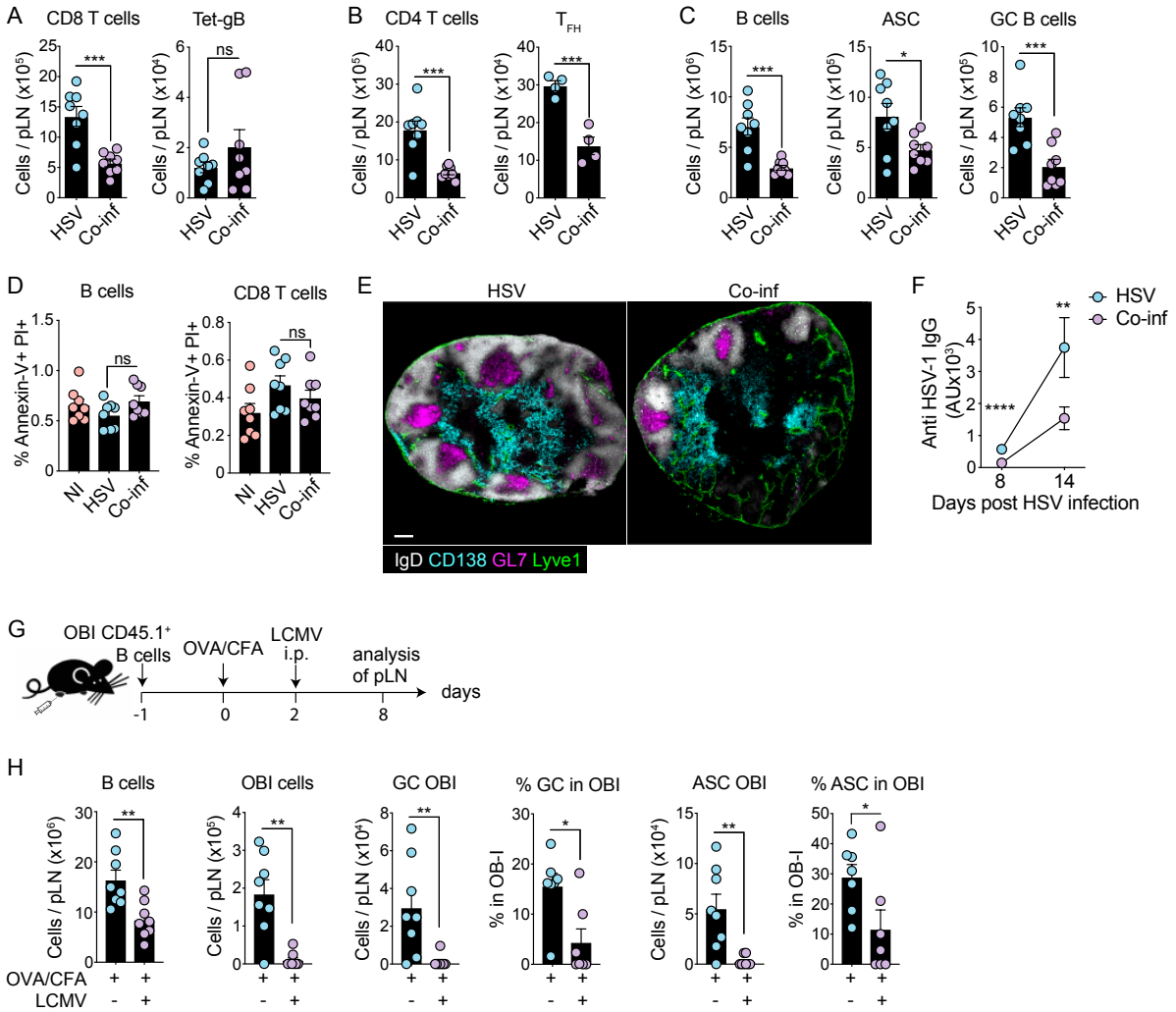

Fig. 4. Systemic coinfection suppresses B cell responses to localized infection. (A-C) Mice were infected as in Fig. 3A and pLN analysed for CD8$^+$ T cells and HSV gB tetramer$^+$ cells (A), CD4$^+$ T cells and CXCR5$^+$ PD1$^+$ CD4$^+$ T_{FH} cells (B) and B cells (C). Graphs show pooled data (mean ± SEM) from 1-2 independent experiments with 4 mice per group. *P < 0.05, *** P < 0.001, ****P < 0.0001, ns, non-significant, by unpaired two-tailed t test. (D) Coinfection does not increase lymphocyte cell death. pLN from HSV and coinfected mice were harvested 5 d post-infection and analysed for Annexin V and PI expression on B and CD8$^+$ T cells by flow cytometry. Inguinal LN from naïve mice were included as controls. Graphs show pooled data (mean ± SEM) from 2 independent experiments with 4 mice per group. ns, non-significant, by ns, non-significant, by unpaired two-tailed t test (E) pLN sections from NI, HSV or LCMV infected mice were stained for IgD, CD138, GL7 and Lyve1 and analysed by confocal microscopy. Data are representative of 2 experiments with 3 mice per group. Scale bar, 200µm. (F) Serum anti–HSV-1 IgG titer assessed by ELISA. Mice were infected as in Fig. 3 and sera harvested at day 8 and 14 post-HSV infection. Graph shows pooled data (mean ± SEM) from 2 independent experiments with 4 mice per group. *P < 0.05, ** P < 0.01, by unpaired two-tailed t test. (G) Experimental schematic. Mice were given CD45.1$^+$ OBI B cells 1 day prior to footpad immunization with OVA/CFA. Mice were infected with LCMV i.p. 2 days later. pLN were analysed 8 d. (H) OBI B cell response in the pLN. Mice were injected i.v. with transgenic OBI-GFP cells and two days later injected s.c. with an emulsion of OVA/CFA. Mice were infected i.p. with LCMV 2 d post immunisation and pLN harvested 8 d post OVA/CFA injection. Graphs show pooled data (mean ± SEM) from 2 independent experiments with 4 mice per group. *P < 0.05, ** P < 0.01, by Mann-Whitney test.

314 *Coinfection-induced lymphopenia suppresses LN expansion and B cell responses*

315 CTL can kill virus infected stromal cells and B cells during infection of mice with strains of
316 LCMV that cause chronic infection[14, 15]. To determine if $CD8^+$ T cells contributed to reduced
317 LN expansion and B cell responses during coinfection with LCMV Armstrong, which is an
318 acute infection, we infected mice with HSV then treated with depleting anti-CD8α antibody
319 prior to LCMV coinfection (Fig. 5A). Suppression of pLN remodelling and impairment of B
320 cell responses in LCMV coinfected mice was unaffected by the loss of $CD8^+$ T cells (Fig. 5B
321 and Fig. S3C). Myeloid cells can also impact B cell responses during chronic LCMV
322 infection[16], but B cell responses were restrained in the dLN of LCMV infected $CCR2^{-/-}$ mice
323 that have defective recruitment of monocytes (Fig. S3D).

324 The reduction in B and T lymphocytes in the pLN of LCMV coinfected mice led us to
325 hypothesize that LCMV infection induces a general lymphopaenia that inhibits lymphocyte
326 recruitment to the draining LN during peripheral viral infection. To examine this, we treated
327 HSV-infected mice with the immunomodulatory drug FTY720 to induce a systemic
328 lymphopenia [17] (Fig. 5C). Expansion of pLN LSC, and upregulation of MAdCAM-1 by FRC
329 was impaired in FTY720 treated HSV infected mice compared to untreated controls (Fig. 5D).
330 B cell accumulation and induction of GC B cells and ASC was also inhibited in FTY720 treated
331 mice, whereas virus-specific $CD8^+$ T cell responses were unchanged, suggesting that
332 lymphopenia impairs the induction of local B cell responses and LN remodelling but not virus-
333 specific $CD8^+$ T cell responses (Fig. 5E).

334 To determine if B cell recruitment was required for expansion of the LN, we treated mice with
335 an anti-CD20 antibody to deplete B cells prior to HSV infection and examined stromal cell and
336 T cell responses in B cell ablated mice (Fig. 5F and Fig. S3E). In the absence of B cells, FRC
337 expansion was significantly reduced and upregulation of MAdCAM-1 by FRC was blunted,
338 whereas LEC and BEC expansion was unaffected (Fig. 5G). T cell recruitment to the HSV-
339 draining pLN and induction of HSV-specific $CD8^+$ T cell responses were unimpaired by
340 depletion of B cells (Fig. 5H). Thus, recruitment of B cells to the dLN during localized viral
341 infection is required to drive FRC expansion, while additional signals contribute to the
342 remodelling of LN endothelial cell compartments.

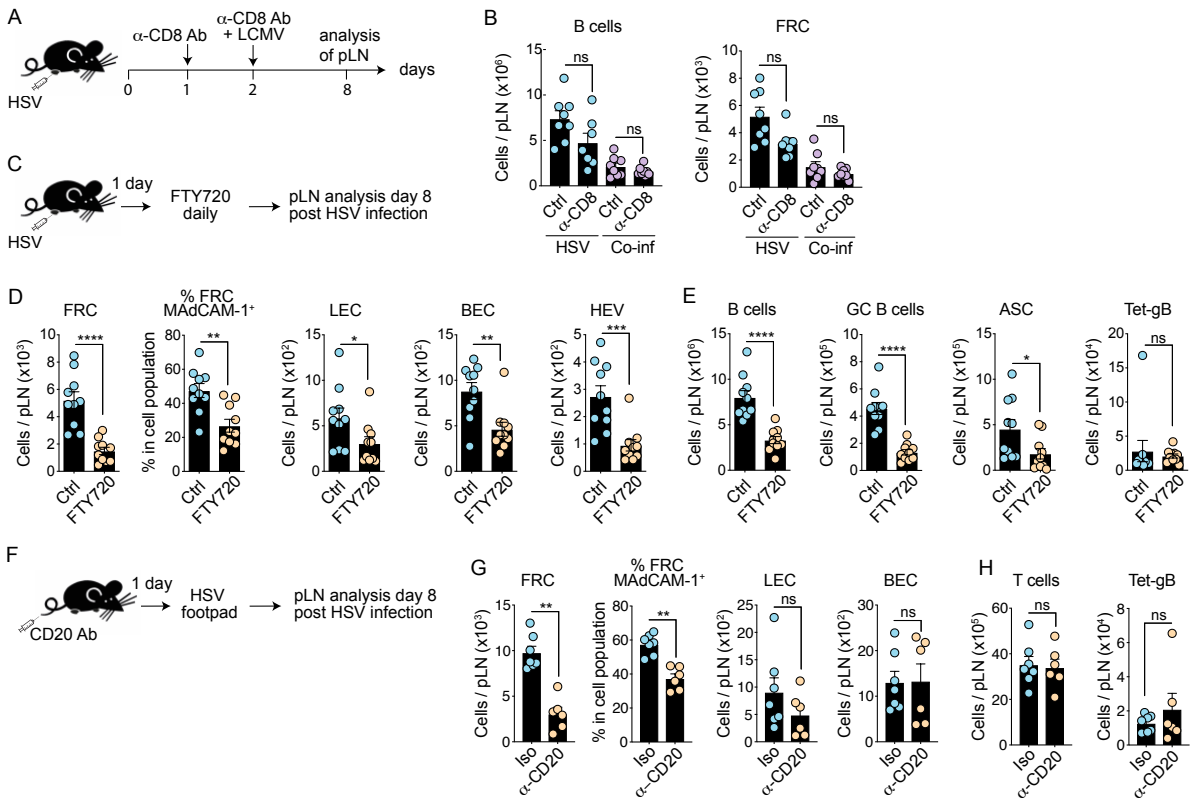

Figure 5. Lymphopenia induced during systemic infection suppresses local LN responses. (A) Experimental schematic of CD8$^+$ T cell depletion during coinfection. Mice were infected s.c. with HSV and injected with CD8 depleting antibody on days 1 and 2. Mice were infected with LCMV on day 2. pLN were analysed 8 d post HSV infection. (B) Numbers of B cells and FRC in the pLN of mice infected with HSV or coinfected with or without CD8$^+$ T cells. Graphs show pooled data (mean ± SEM) from 2 independent experiments with 3-4 mice per group. ns, non-significant, by ANOVA with Krukal-Wallis test. (C) Experimental schematic of FTY720 treatment during HSV infection. Mice were infected s.c. with HSV and the following day injected i.p. with FTY720 or control for 7 d. pLN were analysed 8 d post-HSV infection. (D-E) Absolute numbers of stromal cell subsets and MAdCAM-1 expression on FRC (D), B and T cell responses (E) in pLN of HSV infected mice treated with FTY720. Graphs show pooled data (mean ± SEM) from 2 independent experiments with 5 mice per group. (F) Experimental schematic of B cell depletion during HSV infection. Mice were injected i.p. with CD20 depleting antibody and the following day infected s.c. with HSV. (G-H) Analysis of stromal cells and T cells by flow cytometry in HSV-infected B cell-depleted mice. Graphs show pooled data (mean ± SEM) from 2 independent experiments with 3-4 mice per group. *P < 0.05, **P < 0.01, *** P < 0.001, ****P < 0.0001, ns, non-significant, by Mann-Whitney test (D-E, G-H).

367 *Systemic inflammation suppresses local immunity via IFN-I*

368 We hypothesized that systemic inflammation was responsible for the lymphopenia-induced
369 suppression of local LN responses. To examine this, we administered the TLR agonists
370 poly(I:C) or lipopolysaccharide (LPS) to HSV infected mice (Fig. 6A). Both inflammatory
371 mediators substantially reduced the HSV-driven increase in pLN cellularity, FRC expansion,
372 as well as B cell responses (Fig. 6B). Systemic LCMV infection induces the production of pro-
373 inflammatory cytokines, including type I interferon (IFN-I) [18]. LCMV induced a substantial B
374 cell lymphopenia in mice that was dependent on IFN-I receptor (IFNAR) signalling as it did
375 not occur in IFNAR$^{-/-}$ mice (Fig. 6C). To determine a role for IFNAR signals for suppression
376 of local LN responses, we administered blocking antibodies against IFNAR (anti-IFNAR) to
377 mice infected with HSV or mice coinfected with LCMV in order to reduce IFNAR signals (Fig.
378 6D). Anti-IFNAR treatment did not significantly alter responses in mice infected singly with
379 HSV (Fig. 6E). In contrast, anti-IFNAR blockade significantly enhanced the expansion of FRC,
380 LEC, BEC and HEV in coinfected mice (Fig. 6E and Fig. S4A). HSV-specific T cell responses
381 were not altered by anti-IFNAR treatment (Fig. 6F), but T and B cell recruitment, GC B cells
382 and ASC numbers were restored by anti-IFNAR treatment of coinfected mice (Fig. 6G and Fig.
383 S4A).

384 We asked whether B cell intrinsic IFNAR signals contributed to reduced LN hypertrophy and
385 B cell recruitment during coinfection. We generated chimeric mice with a mixture of B cell
386 deficient (μMT$^{-/-}$) and IFNAR$^{-/-}$ BM to confine the lack of IFNAR expression to B cells (Fig.
387 S4B). However, loss of IFNAR in B cells did not restore LN remodelling or B cell responses
388 in coinfected mice to the levels observed in mice infected with HSV alone (Fig. S4C).
389 Together, these findings show that systemic inflammation during coinfection results in an
390 IFNAR-dependent lymphopenia that reduces cell recruitment to LN draining the site of local
391 infection and impairs LN remodelling and humoral immunity.

392

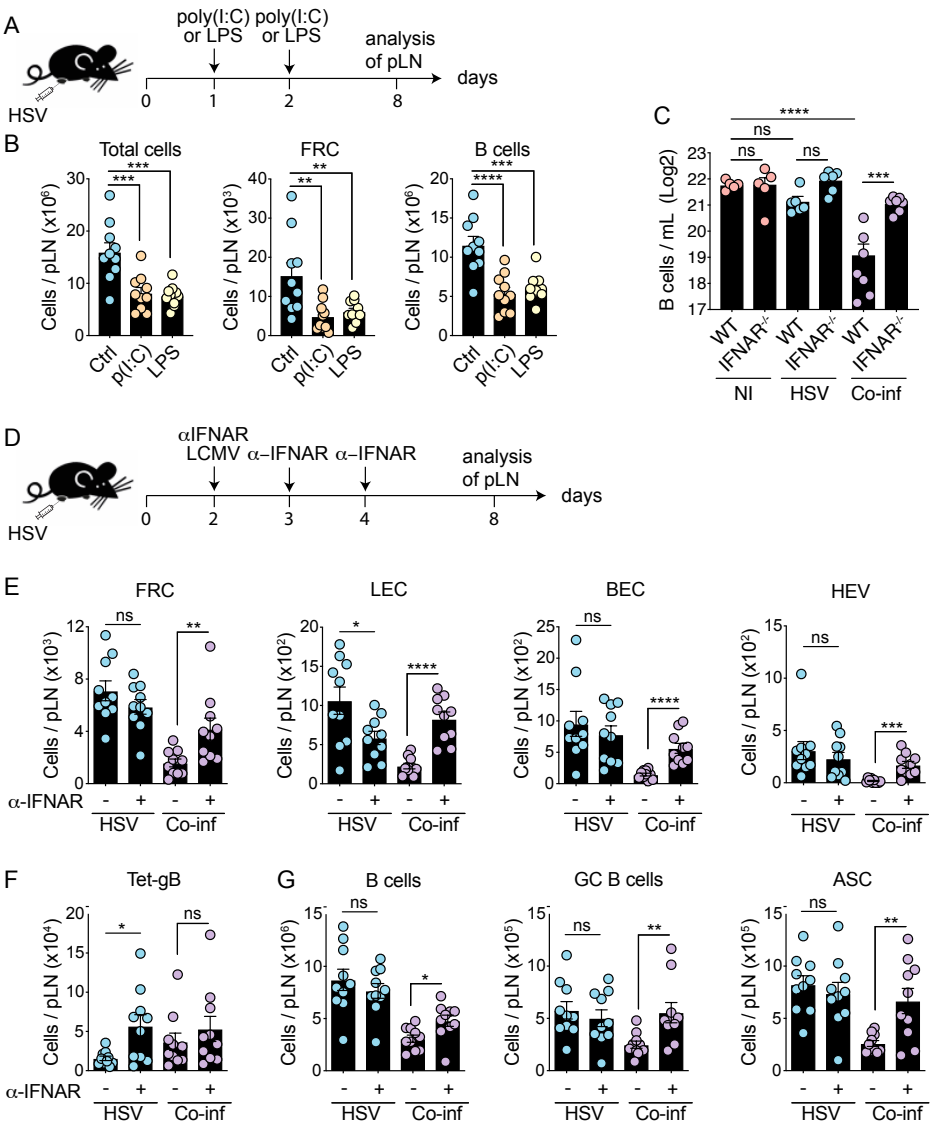

Figure 6. Systemic inflammation suppresses local immunity via IFN-I. (A) Experimental schematic of adjuvant injection in HSV-infected mice. Mice were infected s.c. with HSV and 2 d later received 2 i.p. injections of either poly(I:C) or LPS 24 h apart. pLN were harvested 8 d post-HSV infection. (B) Numbers of total cells, FRC and B cells analysed by flow cytometry in infected mice injected with poly(I:C) or LPS. Graphs show pooled data (mean ± SEM) from 2 independent experiments with 5 mice per group. (C) B cell cellularity in the blood of infected mice. WT or IFNAR KO mice were infected with HSV s.c. and the following day infected with LCMV i.p. Blood was collected on day 3 and B cell numbers analysed by flow cytometry. Graph shows pooled data (mean ± SEM) from 2 independent experiments with 2-4 mice per group. **P < 0.01, *** P < 0.001, ****P < 0.0001, ns, non-significant, by ANOVA with Dunnett's multiple comparisons test (B, C) and Games-Howell's multiple comparisons test (E). (D) Experimental schematic of IFNAR blocking during HSV and coinfection. Mice were infected s.c. with HSV, infected i.p. with LCMV on day 2 and injected with anti-IFNAR blocking antibody or isotype control (ISC) antibody on days 2-4. Mice were analysed on 8 d post-HSV infection. (E-G) Analysis of cellularity of stromal cell subsets (E), HSV-specific $CD8^+$ T cells (F) and B cell response (G) in the pLN of HSV and coinfected mice during IFNAR blocking. Graphs show pooled data (mean ± SEM) from 2 independent experiments with 5 mice per group. *P < 0.05, **P < 0.01, ****P < 0.0001, ns, non-significant, by unpaired two-tailed t test (E-G)

413 **Discussion**

414 Coinfection with multiple pathogens occurs frequently and can alter disease outcomes and
415 subsequent immunity [9, 10]. Diverse mechanisms likely contribute to altered immunity during
416 pathogen coinfections, yet our understanding of these processes remains incomplete. Here, we
417 show that widespread inflammation triggered by systemic coinfection impairs dLN
418 remodelling and B cell responses during localised viral infections or immunization.
419 Mechanistically, systemic inflammation results in a generalized IFN-I-dependent lymphopenia
420 and impairs the recruitment of lymphocytes to LN draining sites of peripheral infection,
421 thereby constraining the induction of local humoral immunity.

422 Many medically important pathogens cause acute or persistent systemic infections, and
423 evidence suggests that immunity to vaccination or challenge with unrelated pathogens is often
424 impaired during coinfection [9, 19]. Models of viral and bacterial coinfection have revealed
425 increased susceptibility to infection and altered responses. During the early stage of LCMV
426 infection, IFN-I sensitizes mice to bacterial endotoxin [18, 20], which can lead to NK cell-mediated
427 impairment of the $CD8^+$ T cell responses [21]. Coinfection of mice with two systemic viral
428 pathogens, LCMV and Ectromelia virus [22] or LCMV and Pichinde virus was also found to
429 impair $CD8^+$ T cell responses to LCMV [23].
430
431 We found that LCMV coinfection did not inhibit HSV-specific $CD8^+$ T cell responses but
432 rather impaired the induction of local B cell responses. In humans, humoral immunity can be
433 impacted during coinfections, although coinfection may both directly and indirectly affect B
434 cell differentiation and antibody production [9]. Bacterial coinfection of mice with *Streptococcus*
435 *pneumoniae* was shown to either enhance or inhibit B cell responses to influenza virus
436 depending on the timing of respiratory coinfection [24]. During the early phase of chronic LCMV
437 infection, virus-specific B cell responses can be inhibited by IFN-I production that results in
438 death of activated B cells and induction of short-lived ASCs at the expense of sustained
439 neutralizing antibody responses [15, 16, 25]. Other viruses also directly interfere with B cell
440 responses via a variety of mechanism [26].
441
442 Here, we describe novel pathway by which coinfection can impede B cell responses. We show
443 that systemic inflammation induced by LCMV infection, the TLR3 agonist Poly(I:C) or the
444 endotoxin LPS induced a lymphopenia that reduced the recruitment of lymphocytes to the dLN
445 during localized infection. This suppression of dLN swelling, stromal cell expansion and B cell

446 immunity suggests that opportunistic localized infections might occur more frequently or be
447 harder to eradicate in hosts undergoing systemic inflammatory reactions. We would also
448 predict that both infectious and non-infectious systemic inflammatory reactions could suppress
449 regional immunity when occuring contemporaneously. In contrast, latent coinfection with
450 murine gammaherpesvirus 68 or murine cytomegalovirus was shown to protect against
451 bacterial infection [27], at least transiently [28], due to the systemic production of low levels of
452 cytokines. This indicates that the magnitude of systemic inflammation can influence the
453 outcomes of immunity.

454 Recruitment of lymphocytes to inflamed LNs triggers LN expansion in response to infection
455 or immunization [4, 29]. This requires circulating lymphocytes as a source of cells to feed the
456 draining LN. Systemic infections and autoimmune diseases including systemic lupus
457 erythematosus (SLE) can induce lymphopenia, resulting in the trapping of lymphocytes in
458 secondary lymphoid organs around the body, thereby reducing the circulating pool of
459 lymphocytes. We show that induction of lymphopenia during systemic infection, inflammation
460 or following FTY720 treatment impairs draining LN responses. B cells can coordinate the
461 expansion of the lymphatic network in LNs during inflammation[30]. We show that removal of
462 B cells impaired the expansion and activation of FRC but had little impact on expansion of
463 LEC or BEC during local HSV infection. The reason for this difference is unclear but may
464 reflect the ability of both $CD4^+$ and $CD8^+$ T cells to also support LN expansion and remodelling
465 [4].

466 Our results show that lymphopenia impairs lymphocyte recruitment and LN remodelling,
467 which impairs B cell responses but does not impact CTL responses. LN hypertrophy peaks 1-
468 2 weeks after infection, whereas T cells are activated and leave the draining LNs within 1 week
469 [31]. Conversely, B cells require a prolonged period of activation and maturation within LN in
470 order to form antibody secreting plasma cells and long-lived memory B cells [32]. This indicates
471 that lymphadenopathy may be critical for the support of B cell responses, probably to support
472 GC reactions and memory B cell formation in the dLN. In support of this, we also observed
473 reduced numbers of T_{FH} cells in coinfected mice. Recruitment of cells to the dLN and
474 expansion of LSC during infection requires IFNAR signalling [4]. Although antibody responses
475 can be enhanced via direct stimulation of T cells by IFN-I [33], we did not find a role for direct
476 IFNAR signalling in B cells. Whether IFNAR signalling on multiple cells types is sufficient to
477 dampen B cell responses during coinfection will require further investigation.

478 Overall, our data show that systemic inflammation impacts remodelling of LN and local B cell
479 responses during localized challenge. It will be important to determine how systemic
480 inflammatory responses in humans impact regional immunity and the progression of diseases
481 that are initiated in barrier tissues.

482

483

484

485 **Methods**

486

487 **Mice.** C57BL/6, B6.SJL-PtprcaPep3b/BoyJ (CD45.1), OBI x B6.129S7-*Rag1*^{tm1Mom}/J
488 (OBI.RAG$^{-/-}$)[34], IFN-αR2$^{-/-}$, B6.129S2-*Ighm*^{tm1Cgn}/J (μMT$^{-/-}$) and B6.129S4-*Ccr2*^{tm1Ifc}/J
489 (CCR2$^{-/-}$) mice were bred in the Department of Microbiology and Immunology. Animal
490 experiments were approved by The University of Melbourne Animal Ethics Committee. All
491 mice were sex and aged matched and used between 8-14 weeks old at the beginning of
492 experiments.

493

494 **Virus infections.** Mice were infected subcutaneously (s.c.) in the footpad with either 5 x 10^4
495 plaque-forming units (PFU) of HSV-1 (KOS) or 2 x 10^4 PFU of LCMV (Armstrong). Mice
496 were infected intranasally with 10^4 of the recombinant influenza virus X31 expressing the HSV
497 glycoprotein-B-derived epitope $gB_{498–505}$ as described[35]. For all infections, mice were
498 anaesthetized with isoflurane vaporized in O_2. Unless stated otherwise mice were coinfected
499 intraperitoneally with 2 x 10^5 PFU of LCMV Armstrong two days after footpad HSV infection.
500 HSV-1 viral titers were determined in homogenized footpads by PFU assay as described[12].

501

502 **Stromal cell isolation and flow cytometry.** pLN and iLN were harvested and processed as
503 described previously[4]. Briefly, LN were teased apart with forceps and incubated at 37°C in
504 RPMI with collagenase D, Dispase and DNase for 25 minutes. Following a second round of
505 digestion for 15 minutes, single cell suspensions were resuspended in FACS buffer (PBS 2%
506 BSA 5mM EDTA) and filtered through 70μM before antibody staining. Antibodies used in
507 this study are listed in Table S1.
508 Live cells were discriminated with a fixable LIVE/DEAD™ Fixable Near-IR Dead Cell Stain
509 Kit (Thermofischer). Annexin V staining was carried out with Annexin V PE and 7AAD from
510 Biolegend according to the manufacturer's instructions.
511 Intracellular staining for KI67 and LCMV were performed using BD Cytofix/Cytoperm™
512 Fixation/Permeabilization Solution Kit according to the manufacturer's instructions. Purified
513 LCMV antibody (Clone VL4, BioXcell) was conjugated to Alexa Fluor™ 594 with antibody
514 labelling kit (ThermoFischer) according to the manufacturer's instructions.
515 Endogenous HSV and LCMV-specific CD8 T cells were identified with H-2Kb-$gB_{498-505}$ and
516 H-2Db-gp_{33-41} (MBL international)-restricted tetramer staining respectively.

517 For metabolism analysis, cells were incubated with Mitotracker Deep Red FM, Bodipy FL C
518 16, CellROX orange reagent or 2-NBDG (all from ThermoFischer) in RPMI supplemented
519 with 10% FCS for 30 minutes at 37°C except for 2-NBDG where glucose-free RPMI
520 (ThermoFischer) was used instead.
521 Cells were enumerated by adding SPHERO calibration particles (BD Biosciences) to each
522 sample before acquisition using FACSCantoII or FACSFortessa (both BD) and Flowjo
523 software was used for analysis.
524
525 **Immunomodulatory treatments.** For $CD8^+$ T cell depletion, mice were injected i.p. twice
526 with 100 µg of anti-CD8 antibody (clone 2.43), 24 hours apart. B cells were depleted with a
527 single injection of 50 µg of anti-mouse CD20 antibody (clone 5D2, Genentech) prior HSV
528 infection. To block lymphocyte egress, FTY720 (2-amino-2-(2-[4-octylphenyl]ethyl)-1,3-
529 propanediol; Cayman chemical, #402616-26-6) was dissolved in 2% cyclodextrin (Sigma) in
530 PBS and i.p. administered daily in mice at a dose of 1mg/kg from day 1 to day 7 post-HSV
531 infection. Control mice were administered with 2% cyclodextrin only. To analyse the effect of
532 systemic inflammation on local immune responses, HSV-infected mice were injected i.p. twice
533 with either 50 µg Polyinosinic:polycytidylic acid high molecular weight (Poly(:IC),
534 InvivoGen) or 5 µg of LPS (Sigma), 24 hours apart. IFNAR in vivo blocking during coinfection
535 was performed by injecting infected mice with 500 µg of anti-IFNAR-1 (clone MAR1-5A3,
536 from BioXcell) or isotype control antibody (clone MOPC-21, BioXcell) for two consecutive
537 days and 250 µg on the third day. Immunization of mice was carried out by injecting 100µg of
538 OVA (Sigma) emulsified in CFA (Sigma) s.c.
539
540 **Generation of bone marrow chimeric mice.** C57BL/6-Ly5.1 recipient mice were lethally
541 irradiated with two doses of 550 rads, 3 h apart, followed by reconstitution with a 80/20 mixture
542 of 8 x 10^6 $\mu MT^{-/-}$ / WT or $\mu MT^{-/-}$ / IFN-$\alpha R2^{-/-}$ donor bone marrow cells and maintained in
543 antibiotic water (neomycin and polymyxin B) for 4 weeks. Recipients were used 8 weeks post-
544 reconstitution.
545
546 **Immunofluorescence and confocal microscopy.** Lymph nodes were harvested and fixed in
547 periodate-lysine-paraformaldehyde (PLP) fixative for 4 hours, incubated in 30% sucrose and
548 embedded in OCT freezing media. LN were harvested and immediately embedded in OCT
549 freezing media. Tissue sections were cut at 16 µm thickness with a cryostat (Leica CM3050S)

550 and air-dried before being fixed in acetone for 5 min, dried, and then blocked for 30 min
551 (Protein Block X0909, DAKO) at room temperature (RT). Sections were staining with primary
552 antibodies for 1 hour at RT, washed in PBS and when required stained with secondary
553 antibodies for 45 minutes at RT. Stained sections were mounted in ProLong Gold antifade
554 reagent (Invitrogen), and acquired on a LSM780 or LSM710 confocal microscope (Carl Zeiss)
555 and images processed with Imaris (Bitplane). Antibodies used for histology are listed in Table
556 S1.
557
558 **Detection of HSV-1 IgG by ELISA.** Nunc MaxiSorp round-bottom 96-well ELISA microtiter
559 plates (Thermo Scientific) were coated overnight at 4°C with 10 µg/ml HSV-1 inactivated Vero
560 cell extract (Advanced Biotechnologies). Unbound protein was washed away (PBS 0.05%
561 Tween20) and serially diluted serum samples (PBS 0.5% BSA) were plated and incubated at
562 RT for two hours. Bound mouse IgG Abs were detected using donkey anti-mouse IgG-HRP
563 and visualized using o-Phenylenediamine. The OD readings were determined at 450/492 nm.
564 Endpoint titers of anti-HSV-1 were calculated by using cut-off values defined as double the
565 OD of non-infected serum control.
566
567 **Statistical analysis.** Graphs and statistics were generated using Prism 8 (GraphPad). Samples
568 were tested for normality and two groups were compared using two-tailed Mann-Whitney U-
569 test or unpaired t-test. Multiple groups were analysed with one-way Anova followed by
570 Tukey's post-test comparison or Kruskal-Wallis, based on Gaussian distribution. All graphs
571 depict means ± SEM.
572
573

574 **Table S1.** Antibodies used for immunofluorescence staining, flow cytometry, blocking and
575 depletion experiments.

Antibody	Clone	Supplier	Application	Fluorochrome
anti-Hamster	Polyclonal	Invitrogen	IF	A647
anti-Rabbit IgG	Polyclonal	Invitrogen	IF	A488
anti-Rabbit IgG	Polyclonal	Invitrogen	IF	A594
anti-Rat IgG	Polyclonal	Invitrogen	IF	A594
B220	RA3-6B2	Biolegend	IF	Pacific Blue
B220	RA3-6B2	Biolegend	FC	PE-Cy7
B220	RA3-6B2	Biolegend	FC	A700
CD138	281-2	BD	FC	PE
CD138	281-2	Biolegend	IF	A647
CD157	BP-3	Biolegend	FC	APC
CD157	BP-3	BD OptiBuild	FC	BV650
CD19	1D3	BD	FC	PerCP/Cy5.5
CD19	1D3	BD	FC	BV605
CD20	5D2	Genentech	depletion	purified
CD31	390	Biolegend	FC	BV421
CD31	MEC13.3	BD	FC	PE
CD31	MEC13.3	Biolegend	IF	A647
CD31	390	ThermoFisher	FC	FITC
CD31	390	Biolegend	FC	Pe-Cy7
CD38	90	Biolegend	FC	PE-Cy7
CD3e	eBio500A2	ThermoFisher	FC	A700
CD4	RM4-5	Biolegend	FC	BV605
CD4	RM4-5	BD	FC	PE-Cy7
CD4	RM4-5	BD	FC	APC
CD45	l3/2.3	Biolegend	FC	A700
CD45	30-F11	BD	FC	PerCP
CD45.2	104	BD	FC	A700
CD8a	2.43	Bio X Cell	depletion	purified
CD8a	53-6.7	Biolegend	FC	BV785
CD8a	53-6.7	Biolegend	FC	APC
CD8b	eBioH35-17.2	ThermoFisher	FC	APC
CD8b	YTS156.7.7	Biolegend	FC	A700
CD8b	H35-17.2	BD	FC	BV785
CXCR5	SPRCL5	ThermoFisher	FC	Biotin
FDCM2	FDC-M2	ImmunoKontact	FC	purified
GL7	GL7	Biolegend	FC	A647
GL7	GL7	Biolegend	IF	Pacific Blue
IFNAR-1	MAR1-5A3	Bio X Cell	blocking	purified
IgD	11-26c.2a	Biolegend	IF	A594
IgG1 isotype control	MOPC-21	Bio X Cell	blocking	purified
KI-67	SolA15	ThermoFisher	FC	eFluor660
Laminin	polyclonal	Abcam	IF	purified
LCMV	VL4	Bio X Cell	FC	purified

Lyve1	polyclonal	Abcam	IF	purified
MAdCAM-1	MECA-367	Biolegend	FC	Biotin
MAdCAM-1	MECA-367	Biolegend	IF	purified
PD1	29F.1A12	Biolegend	FC	PerCP/C5.5
PNAd	MECA-79	ThermoFisher	FC, IF	A488
podoplanin	8.1.1	ThermoFisher	FC	PE
podoplanin	8.1.1	Biolegend	FC	PE-Cy7
podoplanin	8.1.1	Biolegend	IF	purified
podoplanin	8.1.1	ThermoFisher	FC	A488
RANK-L	IK22/5	ThermoFisher	FC	Biotin
Streptavidin		Life Technologies	IF	A555
Streptavidin		BD	FC	APC
Streptavidin		BD	FC	FITC
Streptavidin		BD	FC	PE
Streptavidin		Biolegend	FC	BV711
Streptavidin		BD	FC	PE-Cy7
TCRb	H57-597	BD	FC	BV711
TCRb	H57-597	BD	FC	FITC
TER-119	TER-119	ThermoFisher	FC	PerCP.Cy5.5
TER-119	TER-119	Biolegend	FC	A700

IF, immunofluorescence; FC, flow cytometry

576

577

578

579

580 **Acknowledgments**

581 We thank Hidde Ploegh (Whitehead Institute, Cambridge, MA) for OBI mice, Genentech for
582 anti-mouse CD20 antibody, the Biological Optical Microscopy Platform (BOMP) for
583 support, and Yu Kato for advice on HSV ELISA.

584 **Funding:** This work was supported by the National Health and Medical Research Council of
585 Australia and the Australian Research Council (to LKM, WRH and SNM).

586 **Author contributions:** Conceptualization, YOA and SNM; Methodology, YOA and SD;
587 Investigation, YOA, SD, and SLP; Writing, YOA and SNM; Resources, LKM and WRH;
588 Visualization, YOA and SNM; Funding acquisition, SNM.

589 **Competing interests:** The authors declare no competing interests.

590

591

592 **References**

593

594 1. Alexandre YO, Mueller SN. Stromal cell networks coordinate immune response
595 generation and maintenance. *Immunol Rev* **283**, 77-85 (2018).
596
597 2. Mueller SN, Germain RN. Stromal cell contributions to the homeostasis and
598 functionality of the immune system. *Nat Rev Immunol* **9**, 618-629 (2009).
599
600 3. Malhotra D*, et al.* Transcriptional profiling of stroma from inflamed and resting lymph
601 nodes defines immunological hallmarks. *Nat Immunol* **13**, 499-510 (2012).
602
603 4. Gregory JL*, et al.* Infection Programs Sustained Lymphoid Stromal Cell Responses and
604 Shapes Lymph Node Remodeling upon Secondary Challenge. *Cell Rep* **18**, 406-418
605 (2017).
606
607 5. Mueller SN*, et al.* Regulation of homeostatic chemokine expression and cell trafficking
608 during immune responses. *Science* **317**, 670-674 (2007).
609
610 6. Groom JR*, et al.* CXCR3 chemokine receptor-ligand interactions in the lymph node
611 optimize CD4+ T helper 1 cell differentiation. *Immunity* **37**, 1091-1103 (2012).
612
613 7. Denton AE, Roberts EW, Linterman MA, Fearon DT. Fibroblastic reticular cells of the
614 lymph node are required for retention of resting but not activated CD8+ T cells. *Proc*
615 *Natl Acad Sci U S A* **111**, 12139-12144 (2014).
616
617 8. Cremasco V*, et al.* B cell homeostasis and follicle confines are governed by fibroblastic
618 reticular cells. *Nat Immunol* **15**, 973-981 (2014).
619
620 9. Stelekati E, Wherry EJ. Chronic bystander infections and immunity to unrelated
621 antigens. *Cell Host Microbe* **12**, 458-469 (2012).
622
623 10. Mabbott NA. The Influence of Parasite Infections on Host Immunity to Co-infection
624 With Other Pathogens. *Front Immunol* **9**, 2579 (2018).
625
626 11. Olson MR, McDermott DS, Varga SM. The initial draining lymph node primes the bulk
627 of the CD8 T cell response and influences memory T cell trafficking after a systemic
628 viral infection. *PLoS Pathog* **8**, e1003054 (2012).
629
630 12. Jones CM*, et al.* Herpes simplex virus type 1-specific cytotoxic T-lymphocyte arming
631 occurs within lymph nodes draining the site of cutaneous infection. *J Virol* **74**, 2414-
632 2419 (2000).
633
634 13. Huang HY*, et al.* Identification of a new subset of lymph node stromal cells involved
635 in regulating plasma cell homeostasis. *Proc Natl Acad Sci U S A* **115**, E6826-E6835
636 (2018).
637
638 14. Mueller SN*, et al.* Viral targeting of fibroblastic reticular cells contributes to
639 immunosuppression and persistence during chronic infection. *Proc Natl Acad Sci U S*
640 *A* **104**, 15430-15435 (2007).

641
642 15. Moseman EA, Wu T, de la Torre JC, Schwartzberg PL, McGavern DB. Type I
643 interferon suppresses virus-specific B cell responses by modulating CD8(+) T cell
644 differentiation. *Sci Immunol* **1**, (2016).
645
646 16. Sammicheli S*, et al.* Inflammatory monocytes hinder antiviral B cell responses. *Sci*
647 *Immunol* **1**, (2016).
648
649 17. Halin C*, et al.* The S1P-analog FTY720 differentially modulates T-cell homing via
650 HEV: T-cell-expressed S1P1 amplifies integrin activation in peripheral lymph nodes
651 but not in Peyer patches. *Blood* **106**, 1314-1322 (2005).
652
653 18. Doughty L, Nguyen K, Durbin J, Biron C. A role for IFN-alpha beta in virus infection-
654 induced sensitization to endotoxin. *J Immunol* **166**, 2658-2664 (2001).
655
656 19. Griffiths EC, Pedersen AB, Fenton A, Petchey OL. The nature and consequences of
657 coinfection in humans. *J Infect* **63**, 200-206 (2011).
658
659 20. Nansen A, Randrup Thomsen A. Viral infection causes rapid sensitization to
660 lipopolysaccharide: central role of IFN-alpha beta. *J Immunol* **166**, 982-988 (2001).
661
662 21. Straub T, Freudenberg MA, Schleicher U, Bogdan C, Gasteiger G, Pircher H. Bacterial
663 coinfection restrains antiviral CD8 T-cell response via LPS-induced inhibitory NK
664 cells. *Nat Commun* **9**, 4117 (2018).
665
666 22. McAfee MS, Huynh TP, Johnson JL, Jacobs BL, Blattman JN. Interaction between
667 unrelated viruses during in vivo co-infection to limit pathology and immunity. *Virology*
668 **484**, 153-162 (2015).
669
670 23. Kenney LL, Cornberg M, Chen AT, Emonet S, de la Torre JC, Selin LK. Increased
671 Immune Response Variability during Simultaneous Viral Coinfection Leads to
672 Unpredictability in CD8 T Cell Immunity and Pathogenesis. *J Virol* **89**, 10786-10801
673 (2015).
674
675 24. Wu Y*, et al.* Lethal coinfection of influenza virus and Streptococcus pneumoniae
676 lowers antibody response to influenza virus in lung and reduces numbers of germinal
677 center B cells, T follicular helper cells, and plasma cells in mediastinal lymph Node. *J*
678 *Virol* **89**, 2013-2023 (2015).
679
680 25. Fallet B*, et al.* Interferon-driven deletion of antiviral B cells at the onset of chronic
681 infection. *Sci Immunol* **1**, (2016).
682
683 26. Kuka M, Iannacone M. Viral subversion of B cell responses within secondary lymphoid
684 organs. *Nat Rev Immunol* **18**, 255-265 (2018).
685
686 27. Barton ES*, et al.* Herpesvirus latency confers symbiotic protection from bacterial
687 infection. *Nature* **447**, 326-329 (2007).
688
689 28. Yager EJ*, et al.* gamma-Herpesvirus-induced protection against bacterial infection is
690 transient. *Viral Immunol* **22**, 67-72 (2009).

29. Yang CY, *et al.* Trapping of naive lymphocytes triggers rapid growth and remodeling of the fibroblast network in reactive murine lymph nodes. *Proc Natl Acad Sci U S A* **111**, E109-118 (2014).

30. Angeli V, *et al.* B cell-driven lymphangiogenesis in inflamed lymph nodes enhances dendritic cell mobilization. *Immunity* **24**, 203-215 (2006).

31. Hor JL, Whitney PG, Zaid A, Brooks AG, Heath WR, Mueller SN. Spatiotemporally Distinct Interactions with Dendritic Cell Subsets Facilitates CD4+ and CD8+ T Cell Activation to Localized Viral Infection. *Immunity* **43**, 554-565 (2015).

32. Cyster JG, Allen CDC. B Cell Responses: Cell Interaction Dynamics and Decisions. *Cell* **177**, 524-540 (2019).

33. Le Bon A, *et al.* Cutting edge: enhancement of antibody responses through direct stimulation of B and T cells by type I IFN. *J Immunol* **176**, 2074-2078 (2006).

34. Dougan SK, *et al.* IgG1+ ovalbumin-specific B-cell transnuclear mice show class switch recombination in rare allelically included B cells. *Proc Natl Acad Sci U S A* **109**, 13739-13744 (2012).

35. Davies B, Prier JE, Jones CM, Gebhardt T, Carbone FR, Mackay LK. Cutting Edge: Tissue-Resident Memory T Cells Generated by Multiple Immunizations or Localized Deposition Provide Enhanced Immunity. *J Immunol* **198**, 2233-2237 (2017).

719 **Supplemental Figures**

720

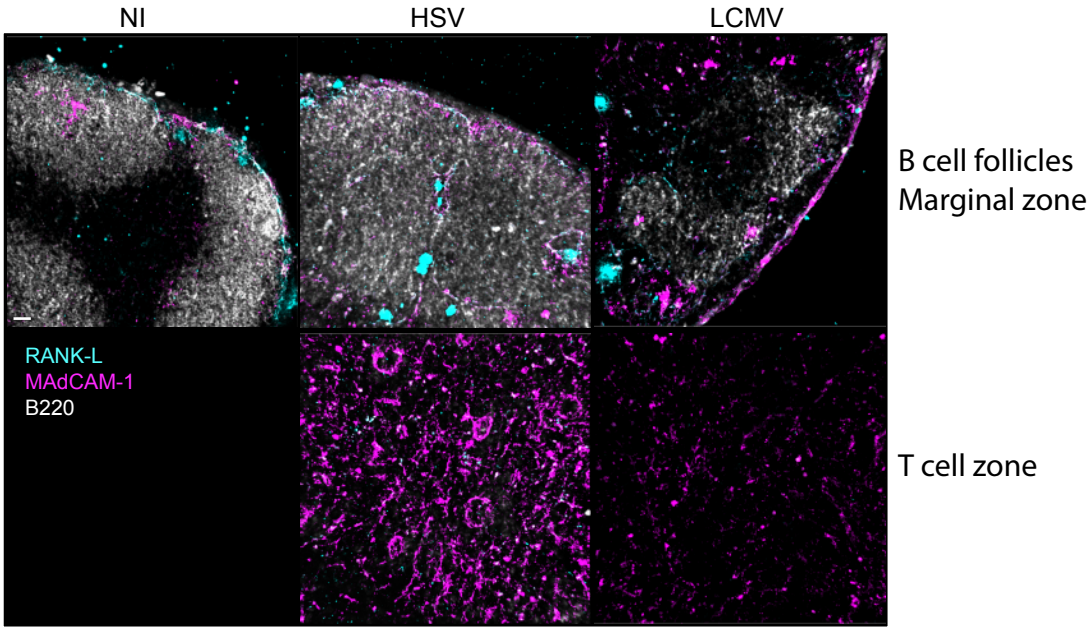

721
722 **Fig. S1. FRC upregulate MAdCAM-1 expression during HSV infection.** pLN sections from
723 NI, HSV or LCMV infected mice were stained for B220, RANK-L and MAdCAM-1, and
724 analysed by confocal microscopy. Data are representative of 2 experiments with 3 mice per
725 group. Scale bar, 40µm.
726

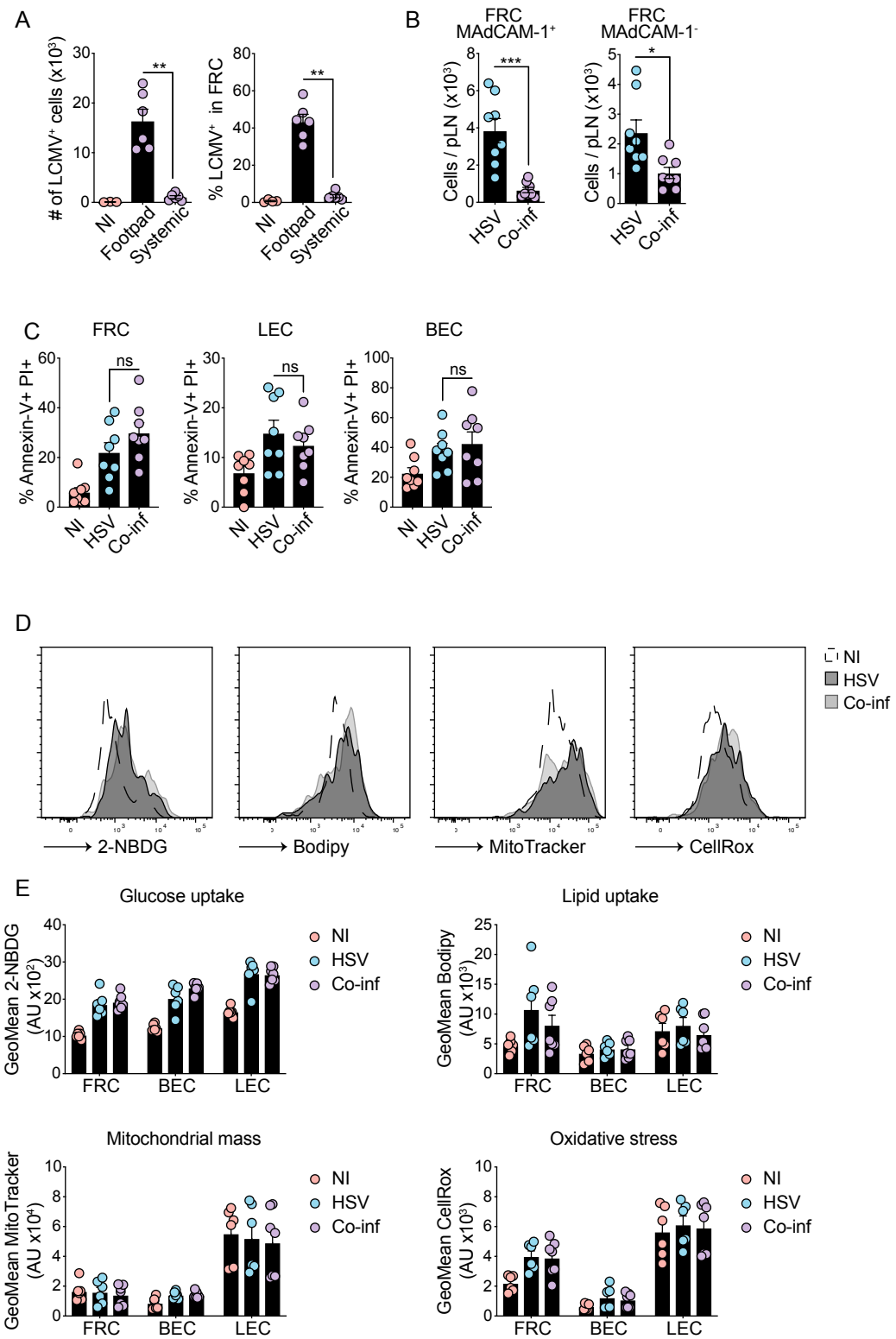

Fig. S2. Systemic coinfection impairs stromal cell expansion. (A) Mice were infected with LCMV s.c. or i.p. and pLN harvested 3 d post-infection. LCMV was detected by intracellular staining and analysed by flow cytometry. Left graph displays total LCMV infected cells, right graph the percentage of infected FRC. Graphs show pooled data (mean ± SEM) from 2 independent experiments with 3 mice per group. **P < 0.01, by Mann-Whitney test (B) Mice were infected with HSV or coinfected as described in Fig. 3. Numbers of FRC expressing or not MAdCAM-1 in pLN were analysed by flow cytometry. Graphs show pooled data (mean ±

735 SEM) from 2 independent experiments with 4 mice per group. *P < 0.05, *** P < 0.001, by
736 unpaired two-tailed t test. (C) pLN from HSV and coinfected mice were harvested 5 d post-
737 infection and analysed for Annexin V and PI expression on stromal cells by flow cytometry.
738 iLN from naïve mice were included as controls. Graphs show pooled data (mean ± SEM) from
739 2 independent experiments with 4 mice per group. ns, non-significant, by by unpaired two-
740 tailed t test (D-E) Metabolism of stromal cells during infection. Mice were infected as in Fig.
741 3 and pLN harvested 8 days post-infection. iLN from naïve mice were used as controls. Cells
742 were incubated with the fluorescent glucose analog 2-NBDG, the fluorescent fatty acid analog
743 BODIPY FL C16, Mitotracker or CellRox before analysis by flow cytometry. Representative
744 histograms on FRC (D) and analysis of geometric mean values on stromal cell subsets (E).
745 Graphs show pooled data (mean ± SEM) from two independent experiments with 3-4 mice per
746 group.
747

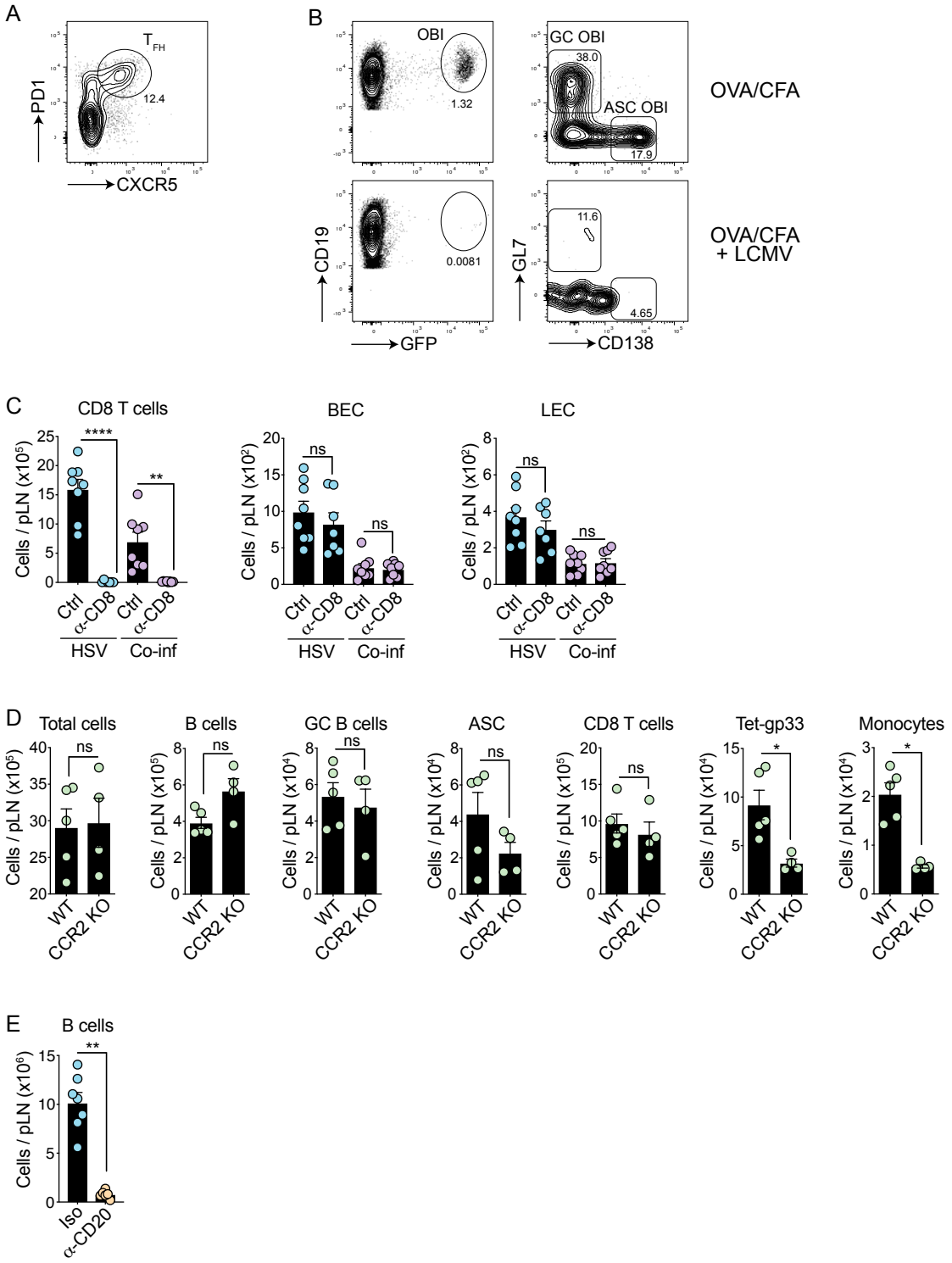

Fig. S3. Lymphopenia suppresses LN expansion and B cell responses.
(A) Gating strategy to identify T_{FH} in infected mice. $CD4^+$ T cells were analysed for CXCR5 and PD1 expression and TFH cells defined as $CD4^+$ $CXCR5^+$ $PD1^+$ cells. (B) OBI B cell response in the pLN. Mice were injected i.v. with transgenic OBI-GFP cells and two days later injected s.c. with an emulsion of OVA/CFA. Mice were infected i.p. with LCMV 2 d post immunisation and pLN harvested 8 d post OVA/CFA injection. Gating strategy to identify OBI cells in the pLN. $CD19^+$ $CD3\varepsilon^-$ B cells were analysed for GFP expression and OBI cells analysed for GL7 and CD138 expression to identify GC OBI and ASC OBI. (C) Experimental

758 procedure as in Fig. 5A. Absolute numbers of $CD8^+$ T cells BEC and LEC in the pLN of mice
759 infected with HSV or coinfected with or without $CD8^+$ T cells. Graphs show pooled data (mean
760 ± SEM) from 2 independent experiments with 3-4 mice per group. **P < 0.01, ****P < 0.0001,
761 ns, non-significant, by ANOVA with Krukal-Wallis test (D) Monocytes are not required for
762 $CD8^+$ and B cell responses during LCMV infection. WT and CCR2 KO mice were infected
763 with LCMV s.c. and pLN harvested 8 d post-infection. B cell and T cell responses were
764 analysed by flow cytometry. Graphs show data from 1 representative experiment out of 2
765 (mean ± SEM) with 4-5 mice per group. (E) B cell depletion following CD20 antibody
766 depleting antibody injection. See Fig. 5F for experimental procedure. *P < 0.05, **P < 0.01,
767 ns, non-significant, by Mann-Whitney test.
768
769

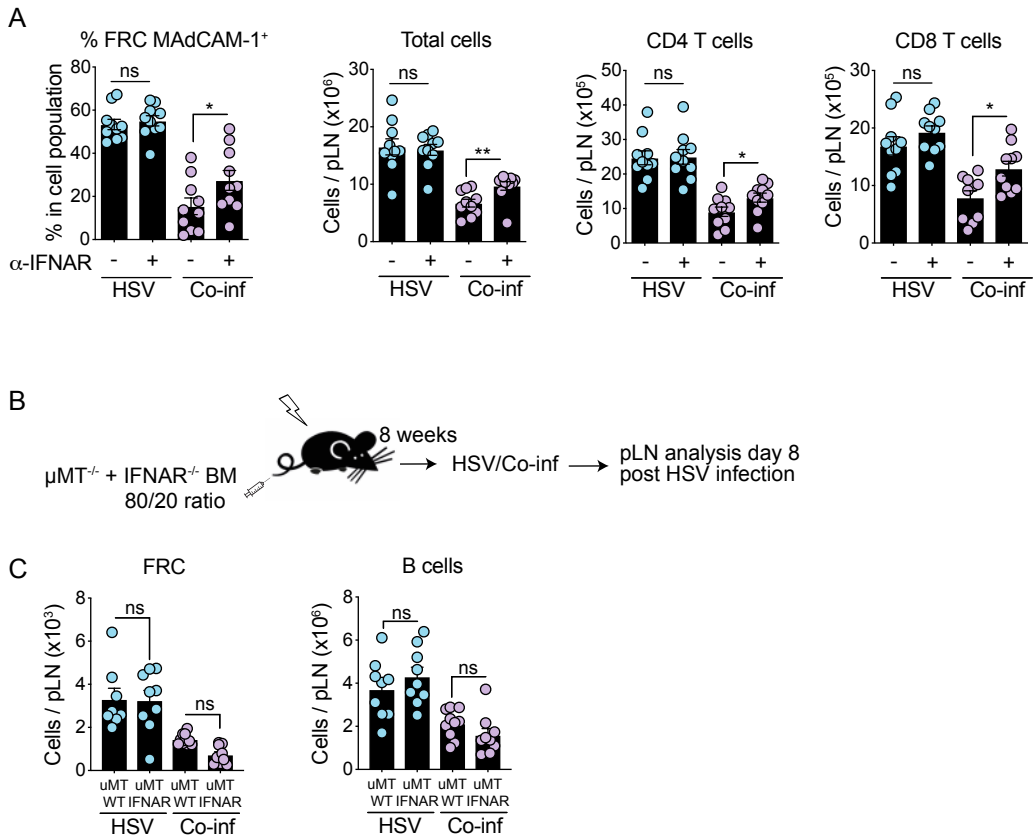

Fig. S4. IFN-I induces local LN suppression via B cell-extrinsic IFNAR signals. (A) Mice were infected as in Fig. 6D. Analysis of cellularity of total cells, HEV, $CD4^+$ and $CD8^+$ T cells in the pLN of HSV and coinfected mice during IFNAR blocking. Graphs show pooled data (mean ± SEM) from 2 independent experiments with 5 mice per group. *P < 0.05, **P < 0.01, ***P < 0.001, ns, non-significant, by unpaired t test (B) Experimental schematic of generating IFNAR deficient B cells. Lethally irradiated mice received a mixture of 80/20 bone marrow cells from μMT + IFNAR or μMT + WT donor mice. 8 weeks post reconstitution, mice were HSV and coinfected as described in Fig. 3A. (C) Absolute numbers of FRC and B cells in the pLN of HSV and coinfected mice in IFNAR B cells deficient mice. Graphs show pooled data (mean ± SEM) from two independent experiments with 4-5 mice per group. *P < 0.05, **P < 0.01, ***P < 0.001, ns, non-significant, by ANOVA with Kruskal-Wallis test.